Acta Biomaterialia 26 (2015) 34–44

Contents lists available at ScienceDirect

Acta Biomaterialia

journal homepage: www.elsevier.com/locate/actabiomat

Elastomeric and mechanically stiff nanocomposites from poly(glycerol sebacate) and bioactive nanosilicates

Punyavee Kerativitayanan [a], Akhilesh K. Gaharwar [a,b,*]

[a] Department of Biomedical Engineering, Texas A&M University, College Station, TX 77843, United States
[b] Department of Materials Science and Engineering, Texas A&M University, College Station, TX 77843, United States

ARTICLE INFO

Article history:
Received 26 April 2015
Received in revised form 28 July 2015
Accepted 18 August 2015
Available online 19 August 2015

Keywords:
Nanocomposites
Elastomer
Poly(glycerol sebacate)
Two-dimensional (2D) silicates
Bone regeneration

ABSTRACT

Poly(glycerol sebacate) (PGS) has been proposed for tissue engineering applications owing to its tough elastomeric mechanical properties, biocompatibility and controllable degradation. However, PGS shows limited bioactivity and thus constraining its utilization for musculoskeletal tissue engineering. To address this issue, we developed bioactive, highly elastomeric, and mechanically stiff nanocomposites by covalently reinforcing PGS network with two-dimensional (2D) nanosilicates. Nanosilicates are ultrathin nanomaterials and can induce osteogenic differentiation of human stem cells in the absence of any osteogenic factors such as dexamethasone or bone morphogenetic proteins-2 (BMP2). The addition of nanosilicate to PGS matrix significantly enhances the mechanical stiffness without affecting the elastomeric properties. Moreover, nanocomposites with higher amount of nanosilicates have higher *in vitro* stability as determined by degradation kinetics. The increase in mechanical stiffness and *in vitro* stability is mainly attributed to enhanced interactions between nanosilicates and PGS. We evaluated the *in vitro* bioactivity of nanocomposite using preosteoblast cells. The addition of nanosilicates significantly enhances the cell adhesion, support cell proliferation, upregulate alkaline phosphates and mineralized matrix production. Overall, the combination of high mechanically stiffness and elastomericity, tailorable degradation profile, and the ability to promote osteogenic differentiation of PGS-nanosilicate can be used for regeneration of bone.

1. Introduction

There are over 2.2 million bone grafting operations worldwide annually, making bone the second most transplanted organs following blood [1,2]. Current clinical gold standard, autograft, provides an optimal osteogenesis, but they are limited in supplies and also result in donor site morbidity [3–5]. Allograft has been increasingly used in the past century due to its availability, but its bone regeneration efficacy is lower than that of autograft and it is also immunogenic [6–8]. The risk of disease transmission can be mitigated by irradiation, but it causes damages to collagen structure, which negatively affects mechanical properties. Due to limitations of autografts and allografts, there is a rising demand for synthetic bone graft substitutes [9–13].

Amongst synthetic bone grafts available in the market, the most successful products are bioactive ceramic granules that surgeons can combine with patient's blood and apply to bone defects as a putty [9–13]. Tricalcium phosphate (β-TCP), hydroxyapatite (HAp), and biphasic calcium phosphate (a mixture of β-TCP and HAp) are the most commonly used because they are similar to calcium-deficient HAp, a natural bone mineral [12]. However, due to lack of control over the degradation rate of these ceramics, it is difficult to mimic the rate of bone healing and regeneration. In the past few years, there has been an increasing interest in bioactive glasses, the silica-based materials composed of Na_2O–CaO–P_2O_5–SiO_2. They are osteoinductive, and have bioactivity index (correlates to the bone-bonding ability) up to 10-folds higher than HAp. In addition, they are class A biomaterials, meaning that they can stimulate bone growth and strongly bond to both bone and soft tissues [12–15]. Despite superior properties, which can fulfill most of the requirements for bone graft substitutes, their brittleness and complex chemistry have limited their translational success. Specifically, bioactive glasses are too brittle for bone defects under cyclic loading and too difficult to cut and shape to fit defect sites [12–15]. Thus, there is a need for alternative materials to control and trigger bone regeneration process.

Recently, a significant interest in design bioactive materials focuses on development of multifunctional nanomaterials [16].

* Corresponding author at: Department of Biomedical Engineering, Texas A&M University, College Station, TX 77843, United States.
E-mail address: gaharwar@tamu.edu (A.K. Gaharwar).

http://dx.doi.org/10.1016/j.actbio.2015.08.025
1742-7061/

It is expected that synergistic interactions between nanomaterials and cells can be used to control and trigger cell fate and can be used to engineer complex tissue structures. We reported the ability of nanosilicate (Laponite – $Na^{+}_{0.7}[(Mg_{5.5}Li_{0.3})Si_8O_{20}(OH)_4]^{-}_{0.7}$) to induce osteogenic differentiation of human mesenchymal stem cells (hMSCs) and adipose stem cells (ASCs) without any osteoinductive supplements such as BMP2 and dexamethasone [15,17]. Nanosilicates are plate-like two-dimensional (2D) nanoparticles composed of salts of silicic acids with a heterogeneous charge distribution [18]. Nanosilicates dissociates into Na^+, Mg^{2+}, Li^+, and $Si(OH)_4$ in aqueous solution. These ionic dissolution products are reported to be involved in cellular adhesion and bone formation. In particular, Mg^+ ions promoted adhesion of osteoblastic cells to materials surfaces via fibronectin receptor $\alpha_5\beta_1$ and β_1 integrins, resulting in enhanced gene expression of ECM proteins and new bone formation [19,20]. Orthosilicic acid or $Si(OH)_4$ promoted synthesis of collagen type I and stimulated osteogenic differentiation [19,21]. Lithium ions (Li^+) were found to activate Wnt/β-catenin signaling which stimulated osteogenic differentiation of mesenchymal progenitor cells, promoted cell proliferation and mineralization, while inhibited apoptosis and osteoclastogenesis [22]. In addition, nanosilicates showed cytotoxicity at ten-fold higher concentration compared to nanohydroxyapatite and silica nanoparticles [15]. Thus, they have promising potentials for bone tissue engineering.

Nanosilicates strongly interacts with hydrophilic polymers such as collagen and poly(ethylene glycol) (PEG), and results in unique property combinations including high stiffness, toughness, bioactivity, and cell adhesion characteristics for biomedical applications [23,24]. Some of the promising biomedical applications for nanosilicates-based composites include high-performance elastomers [25–28], self-healing structures [29], injectable hemostats [30], moldable hydrogels [31], and drug delivery vehicles [32,33]. Recently, our group showed that by incorporating nanosilicates in collagen-based matrix, significant enhances alkaline phosphate (ALP) activity (an early marker for osteogenesis), and promotes production of mineralized matrix [34]. However, the mechanical properties of the collagen-based nanocomposites are significantly lower (modulus ~ 20 kPa) for bone tissue engineering applications and can be used for non-load bearing sites.

Here we report synthesis and fabrication of mechanically stiff and elastomeric nanocomposite from poly(glycerol sebacate) (PGS) reinforced with nanosilicates for bone tissue engineering application. PGS is tough biodegradable elastomeric polyester, synthesized *via* polycondensation of glycerol and sebacic acid [35–37]. The surface eroding nature of PGS makes it preferable for scaffolding application compared to other polyesters. In addition, its degradation products, glycerol and sebacic acid, are bioresorbable; glycerol is a building block for lipid, while sebacic acid is a natural intermediate of fatty acid metabolisms [35,37,38]. Comparing to other widely used synthetic polymers such as poly(lactic acid) (PLA) and poly(lactic-co-glycolic acid)(PLGA)-based materials, PGS triggered lower inflammatory responses and minimal fibrous encapsulation [35–37]. As a consequence, PGS-based scaffolds are explored for various soft tissue engineering applications, including vascular graft [39–41], nerve guide [42], cardiac patch [43], cartilage tissue [44], and retinal transplantation [45]. In addition, it has been reported that PGS supported phenotypes of osteoblasts *in vitro* and was a promising osteoconductive substrate for bone tissue engineering application [46].

To enhance osteogenic capacity of PGS, we propose to incorporate bioactive nanosilicates within the crosslinked PGS network. The addition of nanosilicates to PGS is expected to increase the mechanical stiffness while preserving the elastomeric properties of nanocomposites. Due to the enhanced surface interactions between nanosilicates and PGS, hydrophilicity, biomineralization and physiological stability of nanocomposite network can be improved. We also hypothesize that nanosilicates will improve the cell adhesion characteristics and facilitate *in vitro* mineralized matrix formation. It is anticipated that nanoengineered PGS scaffolds can be used for bone tissue regeneration.

2. Materials and methods

2.1. Poly(glycerol sebacate)(PGS) synthesis

Poly(glycerol sebacate)(PGS) was synthesized by polycondensation of glycerol and sebacic acid (Fig. 1a) according to previously published methods [47]. Glycerol ($C_3H_8O_3$) and sebacic acid ($C_{10}H_{18}O_4$) were obtained from Sigma–Aldrich (USA). Briefly, glycerol and sebacic acid in an equimolar ratio were mixed in a two-neck round-bottom flask, and heated to 120 °C under nitrogen for 24 h. The pressured was then gradually decreased to 50 mTorr, and the reaction was continued for 48 h. The vacuum was turned off and the reactor was filled with Argon. The pre-polymer solution was cooled down to room temperature, transferred to a glass container, and kept in 4 °C refrigerator for future use.

2.2. Synthesis of PGS and PGS-nanosilicate composites

Nanosilicates (Laponite XLG) was obtained from BYK Additives Inc. The nanocomposites were prepared by mixing PGS prepolymer in 70% chloroform–30% ethanol (50% w/v), then adding 0%, 1%, 2.5%, 5%, 10%, 15% w/w of nanosilicates to the PGS (Fig. 1b). Nanosilicates (nSi) were suspended in the solution using a probe sonicator (Model FB120, Fisher Scientific) to uniformly disperse it in PGS prepolymer solution. The increase in viscosity was observed as we add nanosilicates to PGS indicating enhanced interactions between nanoparticle and PGS prepolymer. Then, the solution was poured into a Teflon mold and left in a fume hood for 48 h for solvent evaporation. The dried pre-polymer was put in a vacuum dessicator for 24 h before thermal curing in a vacuum oven at 130 °C for 48 h. The samples were named PGS, PGS-1%nSi, PGS-2.5%nSi, PGS-5%nSi, PGS-10%nSi, and PGS-15%nSi, respectively, according to concentration of nanosilicates.

2.3. Surface morphology

The surface morphology of the nanocomposites was imaged using scanning electron microscopy (FEI Quanta 600 FE-SEM, USA, fitted with an Oxford EDS system). The nanocomposite samples were vacuum dried in a dessicator, then sputter coated with Au/Pd up to a thickness of 8 nm before being mounted onto the specimen stub with carbon tape.

2.4. Sol content analysis

Degree of crosslinking was determined by sol (uncrosslinked network) and gel (crosslinked network) content analysis. Nanocomposites were submerged in THF for 24 h. The swollen samples were dried overnight and the final weight (W_d) was measured. The percentage of sol content (sol%) was calculated from the initial (W_i) and final weight (W_d) using Eq. (1).

$$\text{Sol}\ (\%) = \frac{W_i - W_d}{W_i} \times 1 \quad (1)$$

2.5. Hydration properties

Hydration properties of nanocomposites were evaluated from swelling ratio and contact angle measurement. For the swelling study, samples were submerged in phosphate buffer saline (PBS)

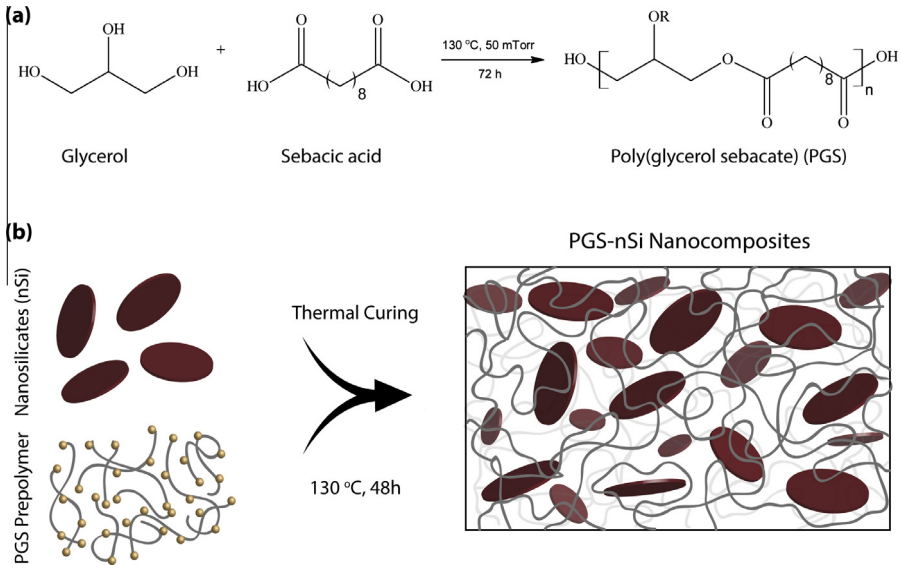

Fig. 1. Synthesis and fabrication of PGS nanocomposites. (a) PGS was synthesized *via* polycondensation of glycerol and sebacic acid. (b) The prepolymer containing PGS and nanosilicate were thermally crosslinked to obtain elastomeric nanocomposites.

at 37 °C for 48 h. The excess surface water was drained and the weight of swollen samples (W_s) was measured. The swelling ratio was calculated from the swollen (W_s) and initial weight (W_i) using Eq. (2). Surface hydrophilicity was determined by water contact angle analysis. A drop of water was dripped onto the sample using a 21-gauge flat needle. The shape of the water drop was captured with a camera (KSV CAM-200 contact angle analyzer, KSV Instruments LTD), and the contact angle was analyzed using imageJ software.

$$\text{Swelling ratio} = \frac{W_s}{W_i} \tag{2}$$

2.6. Degradation studies

Nanocomposites were submerged in phosphate buffer saline (PBS) at 37 °C. The samples were collected after 3, 7, 10, and 28 days, and dried weight was determined. Percentage of weight loss at specific time point was calculated from the initial (W_i) and final dried weight (W_d) using Eq. (3). In complementary to weight loss, surfaces of nanocomposites before (day 0) and after 28 days in PBS (day 28) were imaged using scanning electron microscopy (SEM) (Neoscope JCM-5000).

$$\text{Weight loss } (\%) = \frac{W_i - W_d}{W_i} \times 100 \tag{3}$$

2.7. Thermal analysis

Thermal properties of nanocomposites were determined by thermogravimetric analysis (TGA) (TGA Q50, TA Instruments). The samples weighed ≈10 mg were heated from 0 °C to 750 °C with the heating rate of 10 °C min^{-1}. Thermal stability was determined by calculating the remaining weight at 750 °C. Degradation temperature and temperature range were determined from the first derivative curve (% weight loss/°C).

2.8. Mechanical properties

Since we aimed to use the nanocomposites for bone regeneration at load bearing sites, samples were subjected to cyclic compression using the eXpert 7600, ADMET, USA). Five cycles of loading and unloading were implemented (strain rate 0.1 mm/min). Stress–strain curves were plotted, and compressive modulus, energy loss, and percentage of recovery were calculated. For the fractured surface study, nanocomposites were cut into a thin strip (2 cm long × 0.5 cm wide × 1 mm thick) and pulled vertically (strain rate 0.1 mm/min) until fractured. The fractured surfaces were imaged using scanning electron microscopy to study surface characteristics.

2.9. In vitro biomineralization

Bone bioactivity of nanocomposites was studied by submerging samples in 10× simulated body fluid (10× SBF). SBF was prepared according to previously published methods [48]. Nanocomposites were punched using a 6 mm diameter biopsy punch. The samples were weighed and the volume of SBF needed was calculated accordingly (150 mg/100 ml SBF). The samples were immersed in 10× SBF for 30 min and 6 h, then air dried for further studies. Attenuated Total Reflectance – Fourier Transform Infrared Spectroscopy (ATR-FTIR) (Bruker Alpha FTIR) was used to determine characteristic bands of hydroxycarbonate apatite layer formed on the surface. The samples were further imaged using scanning electron microscopy (SEM). In addition, they were stained by Alizarin Red S (ARS) (2% solution, pH 4.2, Electron Microscopy Sciences) for calcium deposit, and imaged using a stero microscope (Amscope FMA 050). For quantitative analysis, the stained samples were washed in 10% acetic acid (Fisher Scientific) for 30 min with shaking. The solution was neutralized with 10% ammonium hydroxide (Sigma–Aldrich) until the pH fell within the range of 4.1–4.5, then the UV absorbance was read at 405 nm (Infinite M200PRO, TECAN). The absorbance was converted to ARS concentration using a predetermined standard curve.

2.10. Protein adsorption

Protein adsorption on the nanocomposites was determined by washing the samples (6 mm diameter) twice with Dulbecco's phosphate buffered saline (DPBS) before soaking in 10% fetal bovine serum (FBS) at 37 °C for 24 h. DPBS and FBS were purchased from Life Technologies. The samples were washed thrice with DPBS

to remove non-specifically adsorbed proteins. Then, 2% sodium dodecyl sulfate (SDS) solution (20% SDS solution, Amresco) was added with shaking for 6 h to collect adhered protein. The solution was collected and protein concentration was quantified using a Micro BCA™ Protein Assay Kit (Thermo Scientific). Briefly, an equal amount of collected supernatant and BCA working reagent were incubated at 37 °C for 2 h then quantified using a UV/Vis spectrophotometer at 562 nm. The bovine serum albumin (BSA) came with the assay kit was used as a standard.

2.11. In vitro cell adhesion, proliferation and differentiation

MC-3T3 E1 preosteoblasts (ATCC®) were cultured in normal growth media (α-MEM) (Hyclone™) containing 10% fetal bovine serum (FBS) and 1% penicillin/streptomycin (gibco® by Life Technologies), at 37 °C in an incubator with humidified atmosphere (5% CO_2). The cells were used for seeding at 70% confluency in culture. Nanocomposites (6 mm diameter) were glued to a glass slide (1 × 1 cm) with a medical grade silicone adhesive (Loctite 5240), and put into a 24 well plate. The glass slide would aid in handling the samples without disturbing adhered cells. Before cell seeding, the samples were washed twice with DPBS, sterilized under UV light for 4 h, and incubated in normal growth media overnight at 37°c. The cells were trypsinized (0.5% trypsin–EDTA, gibco® by Life Technologies) and seeded on the samples at the high density of 1×10^5 cells in 5 μl normal growth media. The seeded samples were incubated at 37 °C for 3 h to allow cells to adhere; then, 600 μl of normal growth media was added. The samples were collected at 24 h and 3 days after the initial cell seeding. They were washed with DPBS, fixed with 2.5% glutaraldehyde (25% aqueous solution, Alfa Aesar®), and dehydrated with graded ethanol (30%, 50%, 75%, 95%, and 100%, respectively). The seeded samples were then subjected to chemical drying with hexamethyldisilazane (HDMS) (electronic grade, Alfa Aesar®) before sputter coated and imaged with scanning electron microscope.

Preosteoblasts were trypsinized and seeded on pre-conditioned samples at the density of 5000 cells per sample per well (96 well plate) in normal growth media. The samples were divided into 2 sets, the first set was cultured in normal growth media while the other in osteoconductive media (α-MEM supplemented with 10 mM β-glycerolphosphate and 0.05 mM ascorbic acid). β-Glycerolphosphate and ascorbic acid were used as purchased from Sigma–Aldrich. Osteoconductive media was added to the second set of samples at 24 h after the initial cell seeding. Cell proliferation at day 1, 5, 7, 10, and 14 was determined by alamarBlue® assay (Thermo Scientific) following the standard manufacturer's protocol.

Osteogenic differentiation of preosteoblasts was evaluated from determining production of alkaline phosphatase (ALP) and matrix mineralization. ALP was stained by BCIP/NBT solution (Thermo Scientific) at day 3 following the standard manufacturer's protocols. ALP activity was further quantified using SensoLyte® *p*NPP Alkaline Phosphatase Assay Kit, and normalized by amount of double strand DNA (ds-DNA). The amount of dsDNA was quantified using PicoGreen® Assay in conjunction with NanoDrop3300 fluorospectrometer (Thermo Scientific). In addition, matrix mineralization at day 14 was stained by Alizarin Red S, and imaged with the stereomicroscope. The stained images were quantified for the area coverage using ImageJ (NIH) software with Threshold_Colour plugin. For all studies, seeded cells were cultured in normal growth media and osteoconductive media for comparison.

2.12. Statistics

The experimental results are plotted as mean ± standard deviation (n = 3–5). Statistical analysis of all quantitative data was performed by one-way analysis of variance (ANOVA), while pairwise comparison of data was determined by Turkey's post hoc test. Statistical significance was shown as $^{*}p < 0.05$, $^{**}p < 0.01$, $^{***}p < 0.001$.

3. Results and discussion

PGS prepolymer was synthesized *via* polycondensation of glycerol and sebacic acid with molecular weight (M_w) ~ 5012 Da and polydispersity index (PDI) of ~2.6, according to previously published protocol [47]. A fully crosslinked PGS polymer was obtained by thermal curing process at 130 °C for 48 h, according to previously published reports. Different amount of nanosilicates (0%, 1%, 2.5%, 5%, 10%, 15% w/w to the PGS) was incorporated before the thermal crosslinking process to obtain PGS-nanosilicate composites. All the samples were used to evaluate physical and chemical characterization without any post-modification process.

3.1. Nanosilicate enhances crosslinking density and hydrophilicity of nanocomposites

The degree of covalent crosslinking after thermal curing process was determined *via* sol–gel contents. Covalently crosslinked nanocomposites readily swelled in THF and the sol content was leached out. The remaining dry weight of crosslinked network was used to determine the gel content of the nanocomposite network. The results showed that the amount of sol content (uncrosslinked macromer) decreased with increasing nanosilicate concentration, indicating the increase in crosslinking density (Fig. 2a). For example, the sol content was decreased by 15.5% upon the addition of 5% nanosilicates. This ascertained the role of nanosilicates as multifunctional crosslinkers as previously reported [26,31]. Although the exact nature of crosslinking mechanism is not known, but it is expected that the surface of nanosilicate, rich in hydroxyl group, might interact with the hydroxyl group present on PGS backbone to form ester. This resulted in increased gel content due to addition of nanosilicates.

The addition of nanosilicates was expected to increase the swelling ratio of PGS networks as nanosilicates are hydrophilic. The swelling ratios for PGS nanocomposites containing 0%, 1%, 5%, 10%, and 15% nanosilicates were 0.99 ± 0.04, 1.02 ± 0.04, 1.04 ± 0.01, 1.05 ± 0.02, and 1.05 ± 0.03, respectively (Fig. 2b). Additionally, the contact angles of a water droplet on nanocomposites decreased with increasing nanosilicates contents (Fig. 2c). For example, the PGS surface had a water contact angle of 73.9 ± 5.2°, similar to previously reported literature [49]. The addition of 15% nanosilicates lowered the contact angle to 59.7 ± 1.5°, indicating increased in hydrophilicity of nanocomposites. The increase in hydrophilicity was likely due to the polyions present on the nanosilicate surfaces that attracted water molecules and thus, resulted in higher swelling ratio. These properties would affect degradation kinetics as well as cellular responses to the nanocomposites as water molecules at the interfaces influenced protein adsorption and cell adhesion.

To evaluate the effect of nanosilicate on surface properties of nanocomposite, protein adsorption on surface was investigated (Fig. 2d). Proteins adsorbed on the surfaces could affect cell attachment and growth. We soaked the samples in Dulbecco's phosphate buffered saline (DPBS) containing 10% of bovine serum albumin (BSA). The result indicated that the protein adsorbed on PGS and PGS-nanosilicates were twofold more than tissue culture polystyrene (TCP) control. On the other hand, the addition of nanosilicates to PGS had no statistically significant effects on protein adsorption compared to PGS alone.

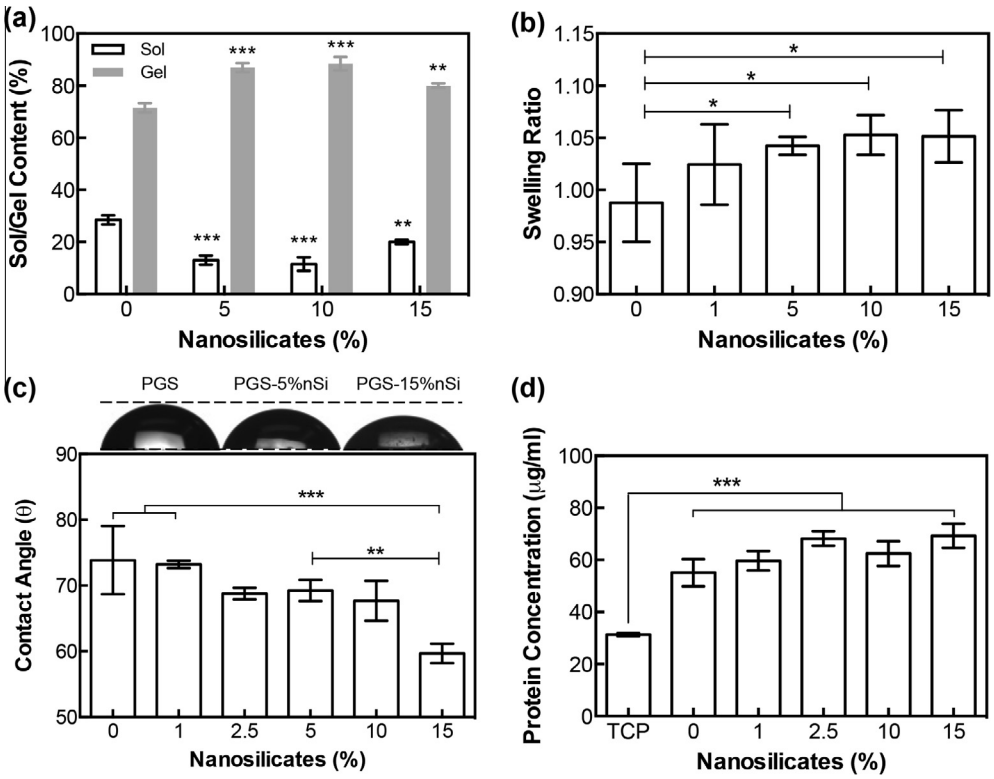

Fig. 2. Effects of nanosilicates on crosslinking density and hydrophilicity. (a) Soluble contents of PGS and PGS-silicates nanocomposites were determined via sol–gel content. Since nanosilicates also acted as crosslinkers, sol fraction significantly decreased upon the addition of nanosilicates compared to PGS. Increases in nanosilicate contents also resulted in (b) higher swelling ratio in physiological conditions and (c) decreased contact angle. (d) However, the addition of nanosilicates had no effects on protein adsorption compared to PGS (statistical significance was shown as $^{*}p < 0.05$, $^{**}p < 0.01$, $^{***}p < 0.001$).

3.2. Nanosilicate improves physiological stability of nanocomposites

Degradation properties of biomaterials have profound effects on their applications in tissue engineering, where scaffolds need to provide structural support while degrading in the rate that matches the rate of new tissue regeneration. Under physiological conditions, PGS degrades by surface erosion *via* cleavage of ester bonds. This is advantageous over bulk-degrading polymers, since PGS exhibits gradual loss in mechanical strength and geometry, in relation to mass loss [35]. After 4 weeks in PBS, the samples were imaged using scanning electron microscope (SEM) to examine the effect of degradation on surface morphology. The images showed that the nanocomposite with higher nanosilicate content underwent significantly less degradation (Fig. 3a). Specifically, for PGS and PGS-1% nanosilicates, a great extent of surface erosion and agglomeration of degraded products were observed. On the other hand, the changes in surface morphology of PGS-10% nanosilicates were minimal.

Degradation profiles of PGS and PGS-nanosilicates nanocomposites were investigated under physiological conditions (PBS, 37 °C) for 4 weeks. From the results, it was apparent that percentage of weight loss significantly reduced with increasing nanosilicate concentrations. For example, on day 10, the weight losses for the samples containing 0%, 5%, 10%, and 15%, were 25 ± 3%, 23 ± 1%, 17.5 ± 2%, and 9.8 ± 1.2%, respectively (Fig. 3b). Statistical analysis revealed significant differences of weight loss upon the addition of nanosilicates for all studied time points (i.e., day 3, 7, and 10). These results indicated that the addition of silicates retarded the degradation of the polyester backbone and enhanced physiological stability by increasing the degree of crosslinking.

It has been reported that nanosilicates disintegrated slowly at pH < 9, while PGS underwent hydrolysis of ester groups and released carboxylic groups. The short-term degradation of PGS and PGS-nanosilcates were mainly dominated by hydrolysis of PGS. A long-term degradation profile involving disintegration of nanosilicates over a period of months will need to be evaluated in the future. Nevertheless, it should be noted that degradation of PGS *in vivo* was reported to be faster than *in vitro* [49]. *In vivo* degradation of PGS was accelerated by esterases present in the surrounding microenvironment.

3.3. Nanosilicate enhances thermal stability of nanocomposites

The thermal characteristics of PGS and PGS-nanosilicates nanocomposites were examined using thermogravimetric analysis (TGA). The samples were heated from 0 to 750 °C with the heating rate of 10 °C min^{-1}. The addition of nanosilicates to PGS network enhanced thermal stability. The remaining weight at 750 °C increased upon the addition of nanosilicates, indicating higher thermal stability (Fig. 4a). For example, pure PGS was completely decomposed at 750 °C, while PGS-15% nanosilicates had 7.2 ± 1.3% weight remained. The first derivative of TGA curves revealed 2-phase thermal degradation profiles (Fig. 4b). The first degradation phase corresponded to the decomposition of crosslinked PGS, at which the temperature was comparable amongst all compositions (approximately 450 °C). The second phase corresponded to a decomposition of crosslinked nanosilicate-PGS networks. The decomposition temperature corresponding to the second phase of thermal decomposition increased with increasing nanosilicate contents. In other words, it took longer time and higher temperature to thermally decompose the crosslinked regions of nanocomposites containing nanosilicates. The results suggested that nanosilicates enhanced thermal stability of the nanocomposites owing to increased degree of crosslinking.

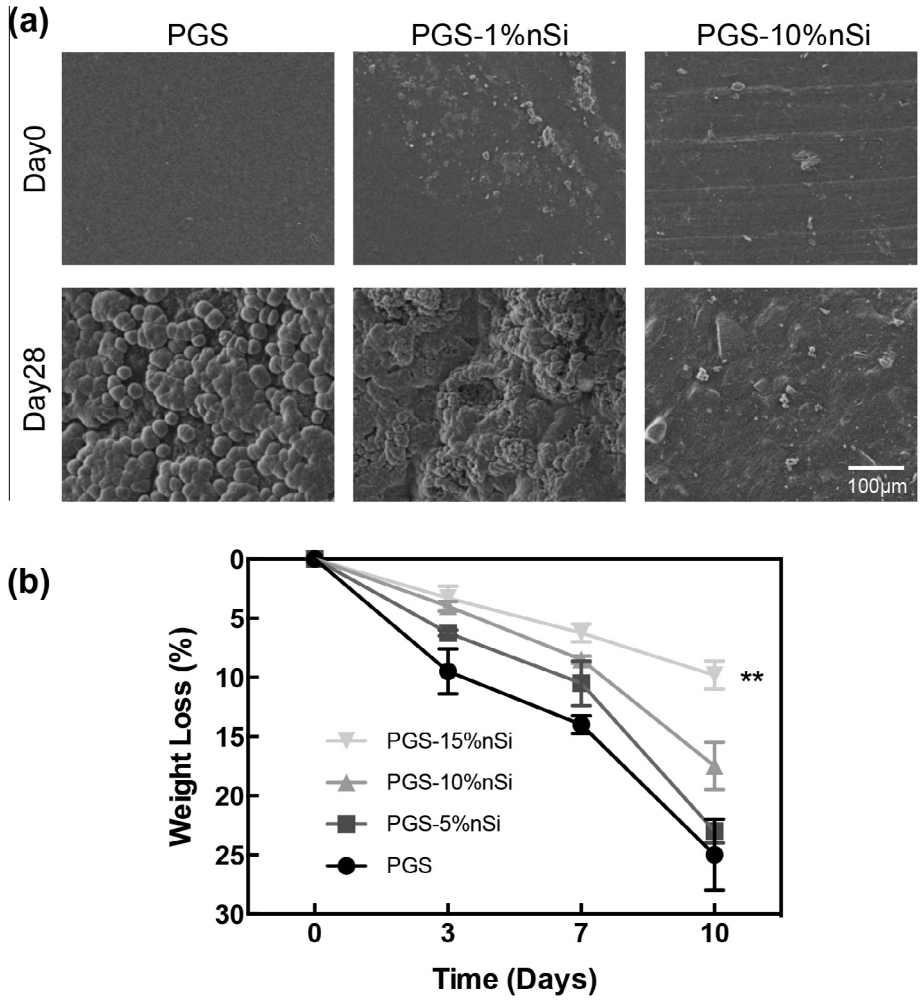

Fig. 3. Effects of nanosilicates on degradation. The addition of nanosilicates to PGS increased the stability of nanocomposites in physiological conditions. (a) For PGS and PGS-1%nanosilicates, agglomerated polymer degradation products were observed all over the surface after 28 days. The nanocomposites with 10% nanosilicate underwent significantly less surface erosion compared to PGS. (b) Percentage weight loss of nanocomposite in PBS decreased with increasing nanosilicate content. Nanocomposite with 15% nSi showed significantly lower weight loss compared to PGS and PGS-5%nSi ($^{**}p < 0.01$).

3.4. Nanosilicate enhances mechanical stiffness of nanocomposites

We aimed to use PGS-nanosilicate nanocomposites for bone regeneration at load bearing sites where they need to withstand repetitive compressive loadings. PGS is an elastomeric polymer and extensively investigated for soft tissue engineering applications [35]. For bone tissue engineering application, the strength and toughness need to be enhanced, ideally to match those of cancellous bone. In addition to osteoinductive properties, nanosilicates has been demonstrated to drastically improve mechanical properties of soft nanocomposite materials [31,33]. So we expect that the addition of nanosilicate to PGS will enhance the mechanical stiffness of nanocomposite network.

To evaluate the elastomeric properties, PGS and PGS-nanosilicate nanocomposites were subjected to 5 cycles of cyclic compression until 20% strain (Fig. 5a). PGS exhibited non-linear stress–strain curve, which is a characteristic of soft elastomeric biomaterials. The stress–strain curve was used to determine the modulus of the crosslinked networks. The compressive modulus of nanocomposite was increased with increasing nanosilicate concentration (Fig. 5b). The modulus was found to be 1.67 ± 1.15 MPa for PGS, which is comparable to literature. The addition of 1%, 2.5%, 5%, and 15% nanosilicates to PGS resulted in 1.93 ± 0.89 MPa, 3.22 ± 0.51 MPa, 6.61 ± 0.27 MPa, and 8.39 ± 0.30 MPa, respectively. The addition of 15% nanosilicates engendered 5-fold increase in compressive modulus. Such enhancements could be attributed to strong interactions between nanosilicate and PGS which restricted movement of polymer chains during deformation and improved load-transfer efficiency within the network.

Energy absorbed by the network during each cycle, and percentage recovery upon cyclic loading, were also determined (Fig. 5c). The maximum energy was absorbed during the first cycle. For subsequent cycles (2–5 cycles), energy absorption was relatively constant for the network. Pure PGS absorbed 5.9 ± 4.4 kJ/m^3 during the first cycle and approximately 2.1 ± 1.6 kJ/m^3 during cycle 2–5. The addition of nanosilicates significantly increased energy absorption, indicating enhanced toughness. For example, during the first cycle nanocomposites containing 1% and 15% nanosilicates exhibited energy absorption of 29.3 ± 5.9 kJ/m^3 and 65.7 ± 3.6 kJ/m^3, respectively. In comparison to PGS, over 11-fold increase in toughness was observed due to the addition of 15% nanosilicates.

Network recovery (%) upon reloading was calculated from the stress–strain curves (Fig. 5d). A crosslinked network of PGS is composed of covalently-linked random coils with hydroxyl groups attached to their backbone. Covalent crosslinks and hydrogen bonds between hydroxyl groups contributed to its elastomericity [35,49]. Interestingly, the addition of nanosilicates resulted in

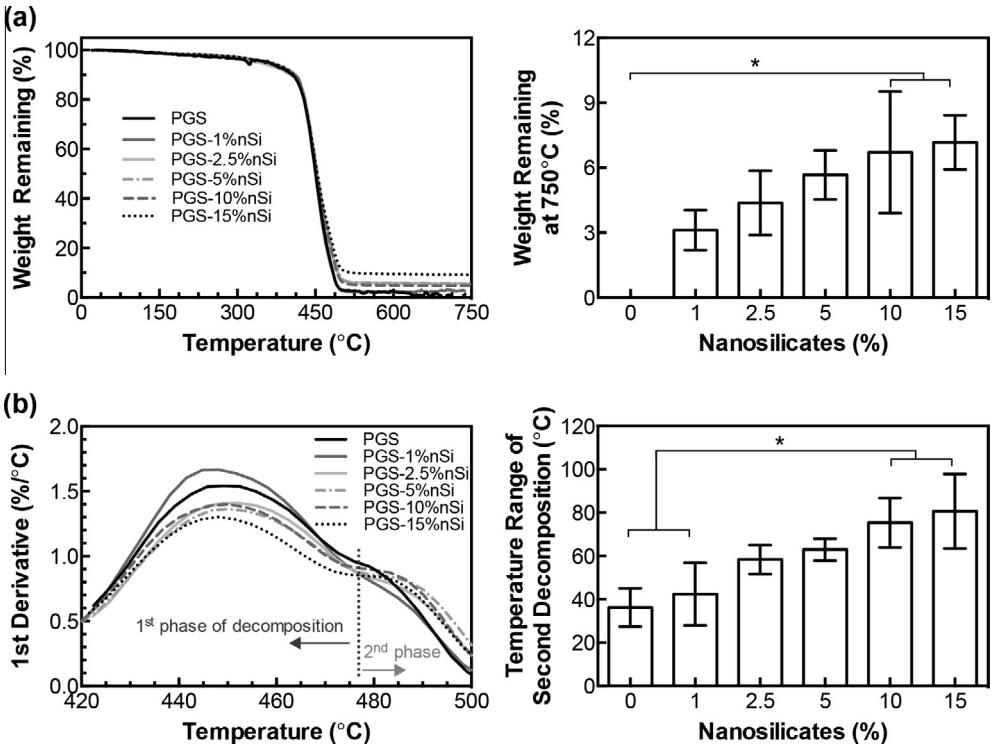

Fig. 4. Effects of nanosilicates on thermal properties. (a) Thermogravimetric analysis indicated the addition of nanosilicates significantly enhanced thermal stability of the networks. (b) The first derivative of the thermograph showed two phases of thermal decomposition. The first phase corresponded to decomposition of the crosslinked PGS network. The temperature range of the second phase, which corresponded to decomposition of PGS-nanosilicate crosslinked networks, increased with increasing silicate content (statistical significance was shown as $^{*}p < 0.05$).

significantly improved mechanical strength and toughness without compromising elastomeric properties of PGS. There was no statistically significant difference between elastic recovery of all PGS and PGS-nanosilicate compositions. For example, the percentage of recovery upon reloading of nanocomposites containing 0%, 5%, and 15% nanosilicates was found to be 85.6 ± 13.6%, 91.9 ± 4.4%, and 93.1 ± 2.0%, respectively. Overall, the addition of nanosilicates to PGS has been shown to enhance energy absorption by 11-fold, increase compressive modulus by 5-fold, while maintaining elastomeric properties of the polymer. These properties of PGS-nanosilicate nanocomposites are promising for bone regeneration at load bearing sites.

As PGS nanocomposite were highly elastomeric, we were not able to observed any fracture until high deformation. In order to complement the cyclic compression tests, we examined the fracture mode of PGS and PGS-nanosilicate composites by subjecting them to a uniaxial tension until break. The fractured surfaces were imaged using scanning electron microscope (SEM) (Fig. 5e). The fractured surface of PGS and PGS-1%nanosilicates showed the forming of stress concentration that eventually led to failure. The surfaces appeared rough and irregular, consisting of microvoids and dimples. These are typical characteristics of ductile fractures where the crack propagates slowly and is accompany by large amount of plastic deformation. PGS nanocomposites with 5% and 10% nanosilicates had smoother fractured surfaces, indicating a shift toward brittle fracture. The fractured surface of PGS-15% nanosilicates displayed a mixture of transgranular and intergranular fractures, which are typically observed in a brittle fracture. Nevertheless, the nanocomposites were able to withstand repetitive loading with almost complete recovery and the surface fractured only after extensive tensile strain ~300%, which is not observed in physiological conditions. So, we did not investigate the tensile characteristics of nanocomposites.

3.5. Nanosilicates enhances in vitro bioactivity

The bone-bonding ability of materials can be evaluated by the ability of hydroxycarbonate apatite (HCA) layer to form on its surface in simulated body fluid (SBF) (Fig. 6a) [50]. HCA is similar to the natural bone mineral, calcium-deficient hydroxyapatite (CDHAp), and is thought to be involved in interaction with collagen fibrils, protein adsorption, and bone progenitor cells' attachment and differentiation [12]. FTIR spectra of PGS submerged in 10× SBF for 6 h contained two weak vibrational bands at 571 and 602 cm^{-1}, which corresponded to the P–O bending of PO_4^{3-} (Fig. 6b). According to the literature, this was an indication that a crystalline phase of HCA had started to develop. Intensities of these two peaks were significantly enhanced for PGS-2.5%nSi soaked in SBF. The spectra of PGS-2.5%nSi also showed a strong band at 1035 cm^{-1} assigned to P–O stretching and a band at 1544 cm^{-1} assigned to C–O stretching of CO_3^{2-}. These phosphate and carbonate bands indicated the formation of a crystalline HCA layer on the nanocomposite surfaces. Comparably, the aforementioned phosphate and carbonate bands were missing in the FTIR spectrum of the PGS and PGS-nSi before submersion in SBF. In addition, the samples immersed in 10× SBF for 30 min were stained for calcium with Alizarin Red S (ARS) dye and quantified (Fig. 6c). It was apparent that the addition of nanosilicates resulted in significantly increased mineralization. For example, more than 3-fold increase in ARS staining was resulted from the addition of 1% nanosilicates. SEM images also showed that hydroxycarbonate apatite (HCA) started to deposit on PGS and PGS-nanosilicate nanocomposites after 30-min immersion in 10× SBF; and the HCA layer developed over time (Fig. 6d). It was apparent that the deposition increased upon the addition of nanosilicate. For example, after 6 h, the surface of PGS-2.5% nanosilicates was almost completely covered by the HCA layer. Overall, these results clearly indicated that

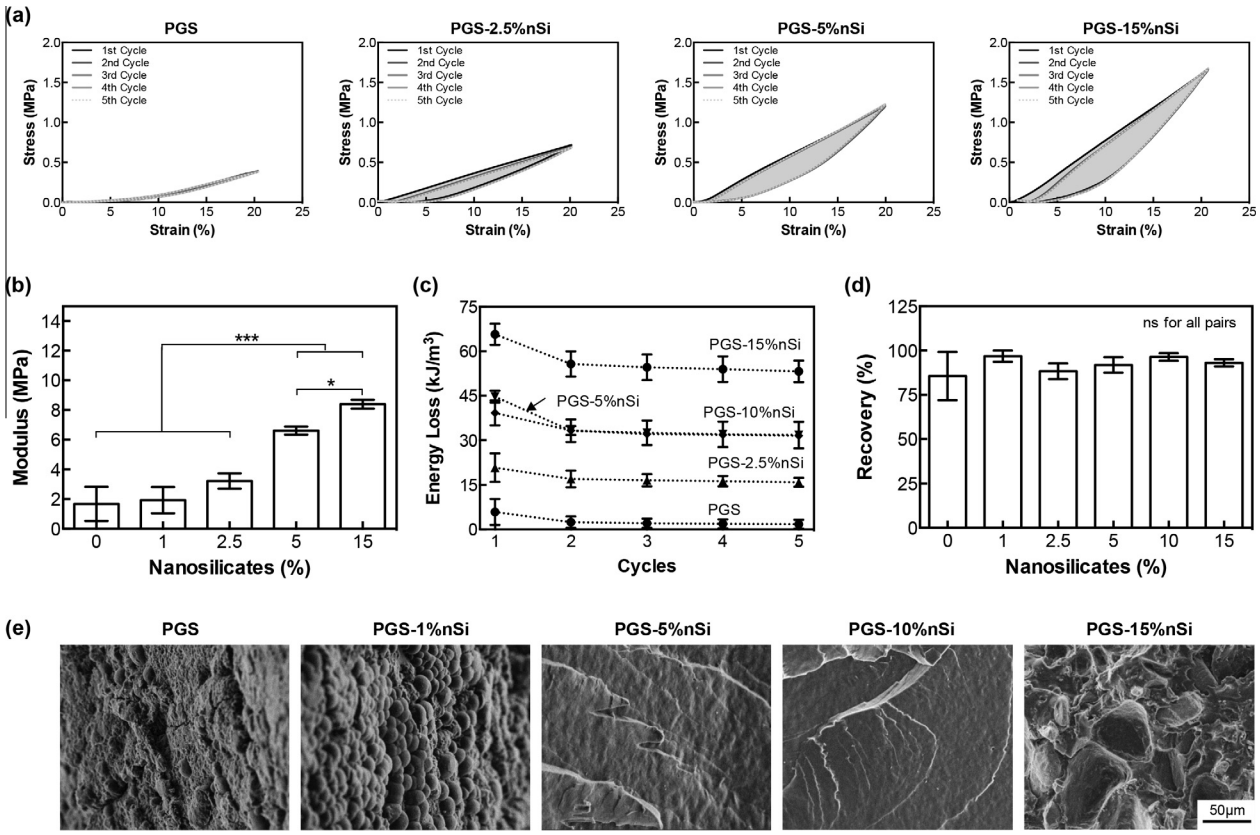

Fig. 5. Effects of nanosilicates on mechanical properties. (a) Cyclic compression of PGS and PGS-nanosilicates nanocomposites. (b) More than 4-fold increase in compressive modulus was observed due to the addition of 10% nanosilicates. (c) Also, nanosilicates enhanced toughness of the networks. The energy absorbed was maximum during the first cycle, and stayed relatively constant in the subsequent cycles. (d) With increased compressive strength, PGS-nanosilicates were able to maintain elastomeric properties, i.e., nanosilicates had no significant effects on % recovery upon reloading. (e) Electron micrographs of fractured surfaces showed ductile fracture of elastomeric PGS, and more brittle-like fractures upon the addition of silicates (statistical significance was shown as $^{*}p < 0.05$, $^{***}p < 0.001$).

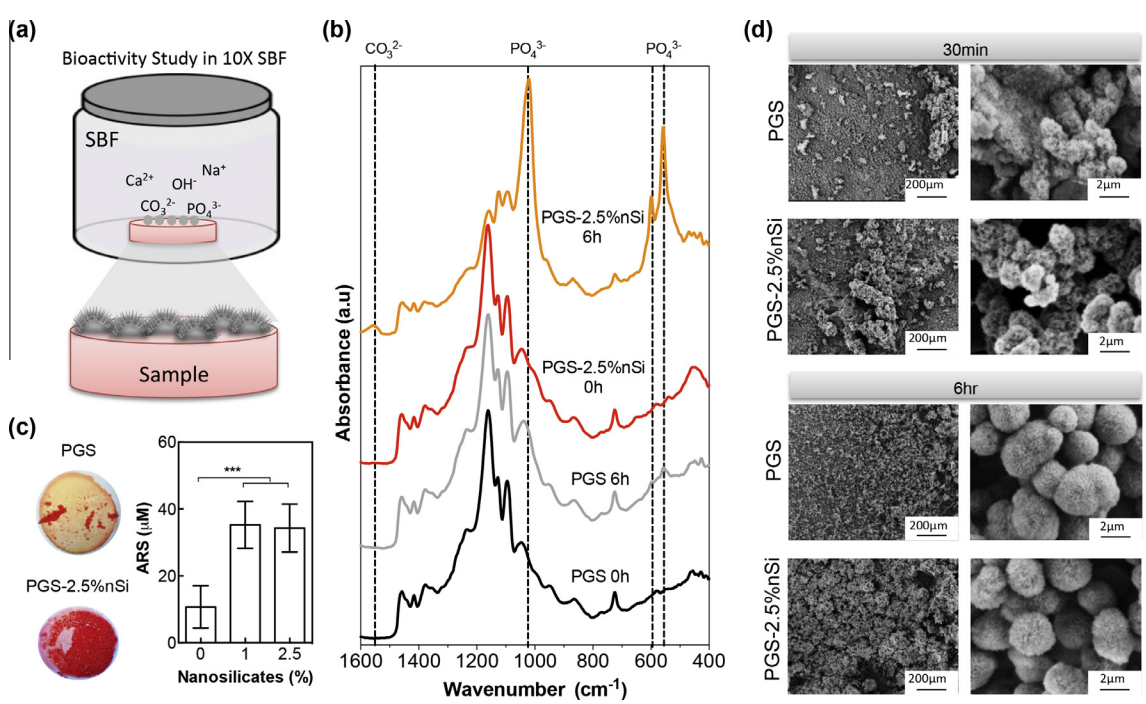

Fig. 6. *In vitro* bioactivity of nanocomposite. (a) The ability of nanocomposite to facilitate hydroxycarbonate apatite (HCA) on the surface was evaluated by subjecting to simulated body fluid (SBF). (b) FTIR spectra showed phosphate and carbonate bands designated to the HCA layer on PGS nanocomposites. The formation of HCA layer increased upon the addition of nanosilicates, as evidenced by (c) Alizarin Red S (ARS) staining for calcium and (d) SEM images. These results suggested that nanosilicates significantly enhanced bone bioactivity of the nanocomposites ($^{***}p < 0.001$).

nanosilicates could significantly enhanced biomineralization, and the PGS-nanosilicates nanocomposites are promising biomaterials for bone regeneration.

3.6. Nanosilicates enhances cell adhesion and proliferation

Initial cell adhesion to biomaterials surface play an important role in cell spreading, proliferation, and differentiation. The pre-osteoblasts cells were seeded on PGS and PGS-silicates and cell adhesion and spreading was evaluated. All substrates supported cell adhesion. Remarkably, cell spreading was enhanced with the addition of nanosilicate, whereas cells on pure PGS appeared spherical (Fig. 7a). This could be attributed to higher surface stiffness or the presence of nanosilicates, or their combinatorial effects. Our earlier reports showed that the addition of nanosilicates to non-fouling and resistant to cell adhesion surfaces (polyethylene glycol (PEG)), resulted in enhanced cell adhesion and spreading [28,51–53]. In a similar study, PNIPAM hydrogels did not support adhesion of fibroblasts and endothelial cells, however, the addition of nanosilicates led to increased cell adhesion in a concentration-dependent manner [33]. It was proposed that nanosilicates provide cell adhesion sites for protein adsorption that subsequently facilitate cell adhesion, however, the actual mechanisms are still unclear.

Proliferation of cells seeded on PGS and PGS-silicates were investigated by analyzing their metabolic activity over two weeks using alamarBlue® assay. All nanocomposite surface supported proliferation of preosteoblasts (Fig. 7b). The metabolic activities of cells increased with time and started to decrease after 1 week of culture. This could be attributed to the cells reaching confluency. Cell proliferation in osteoconductive media was slightly higher than normal growth media; however, there was no statistical difference between the groups. In addition, no significant difference in the metabolic activities was observed due to the addition of nanosilicates. This was opposite to the previous reports that the addition of nanosilicates to PEO resulted in increased metabolic activity in a concentration-dependent manner [52]. This discrepancy could be explained by the fact that PEO exhibited low cell attachment, thus, significant enhancement was observed upon the addition of nanosilicates. On the other hand, PGS itself is cell adhesive, and has been demonstrated in the literature to be cytocompatible and support cell proliferation. From the metabolic activity study, it was evidenced that cell proliferation on PGS and PGS-nanosilicates were higher on TCP during the first week and vice versa in the second week, unlike the PEO-nanosilicates system in which cell proliferation on the nanocomposites with 70% nanosilicates was still significantly lower than TCP.

3.7. Differentiation of preosteoblasts on PGS and PGS-nSi

The ability of PGS-nanosilicate nanocomposites to promote osteogenesis was determined by assessment of ALP and matrix mineralization production by the seeded cells in both normal growth and osteoconductive media (αMEM supplemented with β-glycerophosphate and ascorbic acid). As an early marker of osteogenic differentiation, ALP staining and subsequent image quantification was performed on day 3. In both media conditions, PGS-nSi nanocomposites displayed stronger ALP staining compared to PGS (Fig. 8a). The quantification of ALP activity further confirmed the results. There was no apparent difference in the staining between the normal growth and the osteoconductive groups at this time point. The increases in ALP activity with the

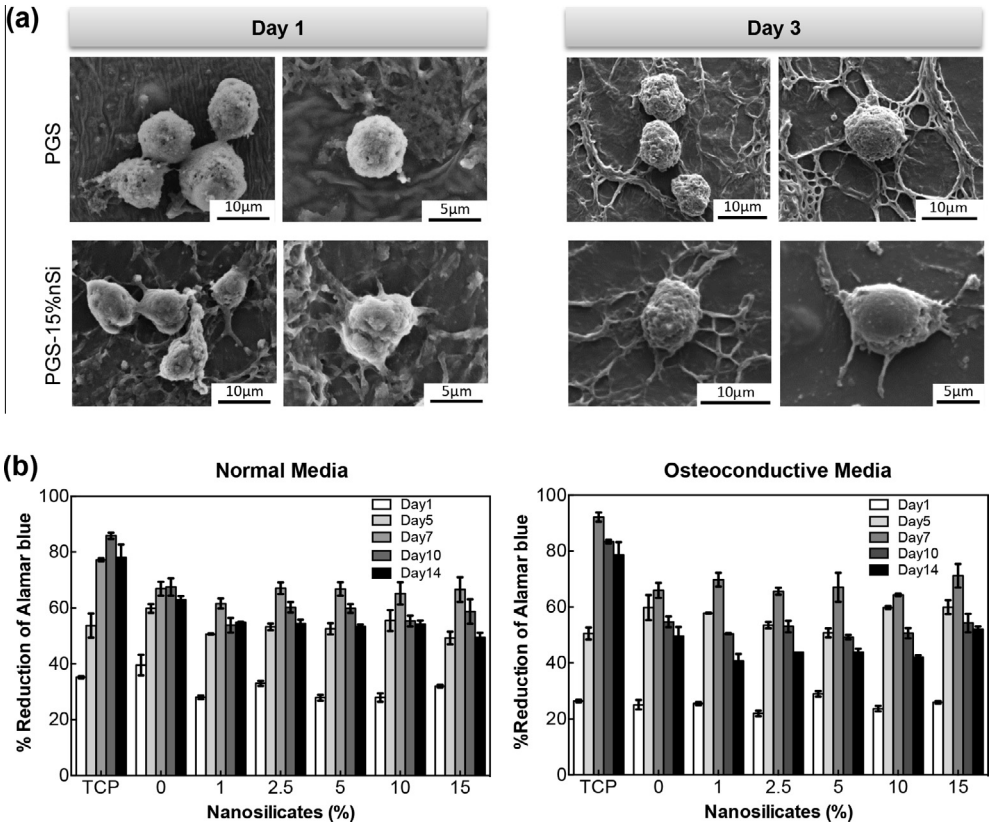

Fig. 7. Cellular adhesion and proliferation on nanocomposites. (a) PGS and PGS-nanosilicates supported initial cell adhesion. The cell spreading increased upon the addition of nanosilicates. (b) Both PGS and nanocomposite supported cell proliferation over a period of 14 days and no significant difference was observed between the groups.

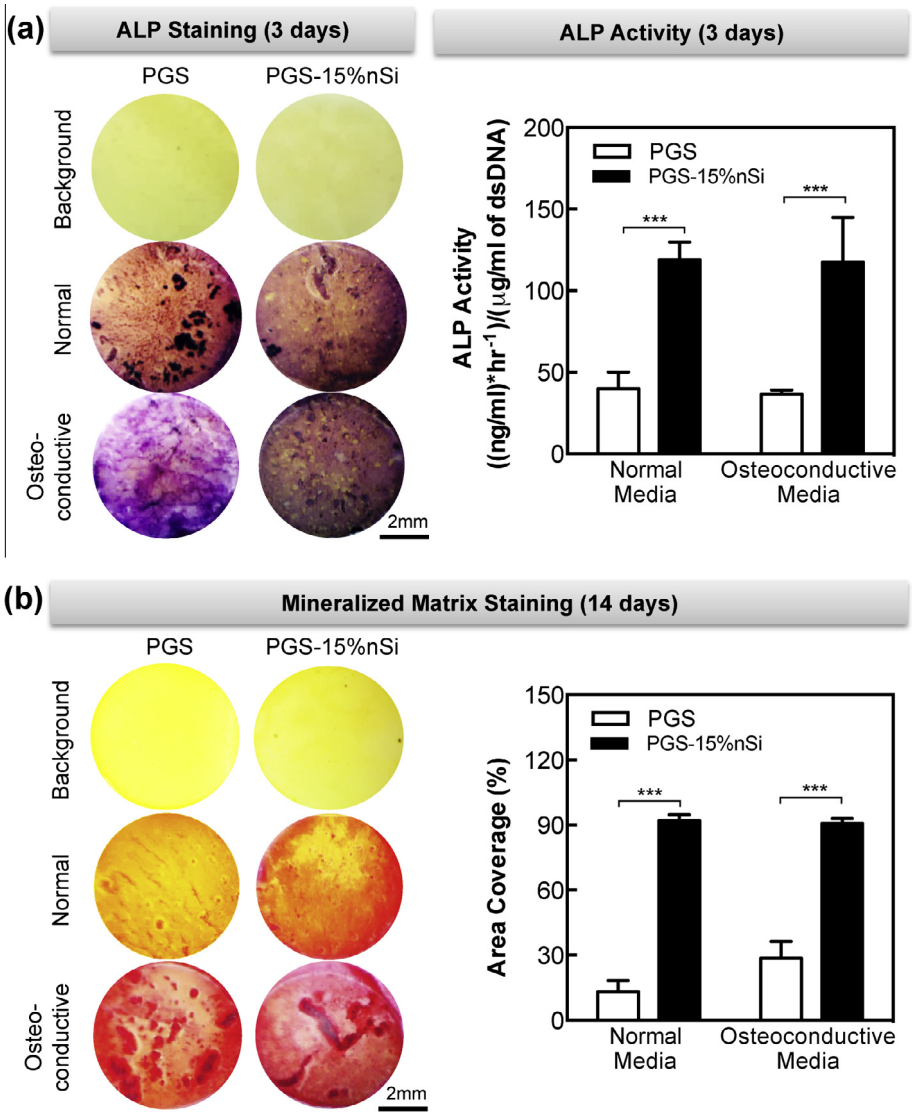

Fig. 8. Differentiation of preosteoblasts on PGS nanocomposites. The addition of nanosilicates enhanced osteogenic differentiation of seeded cells as evidenced by (a) increased alkaline phosphatase (ALP) activity on day 3 and (b) increased matrix mineralization on day 14. The images of stained samples were quantified and plotted (right figures). Also, it should be note that matrix mineralization in osteoconductive media was significantly higher than that in normal media ($^{***}p < 0.001$).

addition of nanosilicates indicated a key role of nanosilicates in upregulating osteogenic differentiation.

Furthermore, matrix mineralization, a late-stage marker of osteogenic differentiation, was assessed on day 14 by ARS staining. The addition of nanosilicates resulted in significant increases in ARS staining in a concentration-dependent manner (Fig. 8b). Moreover, the samples in osteoconductive media displayed higher ARS staining compared to the cells seeded in normal growth media. Image quantification showed more than 6-fold increase in percentage of area coverage upon the addition of 15% nanosilicates when cultured in normal growth media. It is important to note that the enhancement of both ALP activity and matrix mineralization with increasing nanosilicate concentrations were observed in the absence of osteogenic factors such as BMP2 and dexamethasone. In particular, nanosilicates promoted ALP and mineralized matrix deposition even when the preosteoblasts were cultured in normal growth media. In a summary, the results indicated that nanosilicates could promote osteogenic differentiation of preosteoblasts without any osteogenic factors. These agreed with previous works reporting osteoinductive properties of nanosilicates [15,34].

4. Conclusion

We successfully fabricated PGS-nanosilicates elastomeric nanocomposites. Degree of crosslinking, hydrophilicity, thermal and structural stability can be tailored by addition of nanosilicate. Importantly, mechanical strength and stiffness could be enhanced while the elastomeric property of the polymer was still preserved. *In vitro* mineralization also showed increased bioactivity upon the addition of nanosilicates. The nanocomposites supported attachment and proliferation of preosteoblasts and significantly promoted osteogenic differentiation of cells in the absence of osteogenic factors, suggesting osteoinductive properties of the nanocomposites. Overall, these indicate that PGS-nanosilicate nanocomposites can be used for bone tissue engineering applications.

Disclosures

All of the authors declared no conflict of interest regarding publication of this paper.

Acknowledgments

We would like to thank Alpesh Patel and Teena Thakur for help with PGS synthesis and false colored SEM images used in the table of content, respectively. We would also like to thank Prof. Melissa A. Grunlan for providing access to thermal analysis equipment and technical feedback.

References

[1] P.V. Giannoudis, H. Dinopoulos, E. Tsiridis, Bone substitutes: an update, Injury 36 (2005) S20–S27.
[2] G. Grabowski, C.A. Cornett, Bone graft and bone graft substitutes in spine surgery: current concepts and controversies, J. Am. Acad. Orthop. Surg. 21 (2013) 51–60.
[3] H.C. Pape, A. Evans, P. Kobbe, Autologous bone graft: properties and techniques, J. Orthop. Trauma 24 (2010) S36–S40.
[4] J.T. Marino, B.H. Ziran, Use of solid and cancellous autologous bone graft for fractures and nonunions, Orthop. Clin. North Am. 41 (2010) 15–26.
[5] U. Kneser, D. Schaefer, E. Polykandriotis, R. Horch, Tissue engineering of bone: the reconstructive surgeon's point of view, J. Cell Mol. Med. 10 (2006) 7–19.
[6] C. Myeroff, M. Archdeacon, Autogenous bone graft: donor sites and techniques, J. Bone Joint Surg. 93 (2011) 2227–2236.
[7] G. Zimmermann, A. Moghaddam, Allograft bone matrix versus synthetic bone graft substitutes, Injury 42 (2011) S16–S21.
[8] E.M. Younger, M.W. Chapman, Morbidity at bone graft donor sites, J. Orthop. Trauma 3 (1989) 192–195.
[9] M. Bohner, Resorbable biomaterials as bone graft substitutes, Mater. Today 13 (2010) 24–30.
[10] A.S. Greenwald, S.D. Boden, V.M. Goldberg, Y. Khan, C.T. Laurencin, R.N. Rosier, Bone-graft substitutes: facts, fictions, and applications, J. Bone Joint Surg. 83 (2001) S98–S103.
[11] T. Blokhuis, J.C. Arts, Bioactive and osteoinductive bone graft substitutes: definitions, facts and myths, Injury 42 (2011) S26–S29.
[12] J.R. Jones, Review of bioactive glass: from Hench to hybrids, Acta Biomater. 9 (2013) 4457–4486.
[13] C. Seebach, J. Schultheiss, K. Wilhelm, J. Frank, D. Henrich, Comparison of six bone-graft substitutes regarding to cell seeding efficiency, metabolism and growth behaviour of human mesenchymal stem cells (MSC) in vitro, Injury, Int. J. Care Injured 41 (2010) 731–738.
[14] R. Detsch, H. Mayr, G. Ziegler, Formation of osteoclast-like cells on HA and TCP ceramics, Acta Biomater. 4 (2008) 139–148.
[15] A.K. Gaharwar, S.M. Mihaila, A. Swami, A. Patel, S. Sant, R.L. Reis, et al., Bioactive silicate nanoplatelets for osteogenic differentiation of human mesenchymal stem cells, Adv. Mater. 25 (2013) 3329–3336.
[16] P. Kerativitayanan, J.K. Carrow, A.K. Gaharwar, Nanomaterials for Engineering Stem Cell Responses, Adv. Healthc. Mater. 4 (2015) 1600–1627.
[17] S.M. Mihaila, A.K. Gaharwar, R.L. Reis, A. Khademhosseini, A.P. Marques, M.E. Gomes, The osteogenic differentiation of SSEA-4 sub-population of human adipose derived stem cells using silicate nanoplatelets, Biomaterials 35 (2014) 9087–9099.
[18] D. Chimene, D. Alge, A.K. Gaharwar, Two-dimensional nanomaterials for biomedical applications: emerging trends and future prospects, Adv. Mater. (2015), http://dx.doi.org/10.1002/adma.201502422.
[19] A. Hoppe, N.S. Güldal, A.R. Boccaccini, A review of the biological response to ionic dissolution products from bioactive glasses and glass-ceramics, Biomaterials 32 (2011) 2757–2774.
[20] H. Zreiqat, C.R. Howlett, A. Zannettino, P. Evans, G.C. Schulze-Tanzil, M.S. Knabe, Mechanisms of magnesium-stimulated adhesion of osteoblastic cells to commonly used orthopaedic implants, J. Biomed. Mater. Res. 62 (2002) 175–184.
[21] D.M. Reffitt, N. Ogston, R. Jugdaohsingh, H.F.J. Cheung, B.A.J. Evans, R.P.H. Thompson, et al., Orthosilicic acid stimulates collagen type 1 synthesis and osteoblastic differentiation in human osteoblast-like cells in vitro, Bone 32 (2003) 127–135.
[22] T. Kubota, T. Michigami, K. Ozono, Wnt signaling in bone metabolism, J. Bone Miner. Metab. 27 (2009) 265–271.
[23] A.K. Gaharwar, N.A. Peppas, A. Khademhosseini, Nanocomposite hydrogels for biomedical applications, Biotechnol. Bioeng. 111 (2014) 441–453.
[24] J.K. Carrow, A.K. Gaharwar, Bioinspired polymeric nanocomposites for regenerative medicine, Macromol. Chem. Phys. (2014).
[25] P. Podsiadlo, A.K. Kaushik, E.M. Arruda, A.M. Waas, B.S. Shim, H.N. Jiadi Xu, et al., Ultrastrong and stiff layered polymer nanocomposites, Science (2007) 318.
[26] A.K. Gaharwar, C.P. Rivera, C.-J. Wu, G. Schmidt, Transparent, elastomeric and tough hydrogels from poly(ethylene glycol) and silicate nanoparticles, Acta Biomater. 7 (2011) 4139–4148.
[27] L.J. Bonderer, A.R. Studart, L.J. Gauckler, Bioinspired design and assembly of platelet reinforced polymer films, Science (2008) 319.
[28] A.K. Gaharwar, P. Schexnailder, V. Kaul, Ozan. Akkus, D. Zakharov, S. Seifert, et al., Highly extensible bio-nanocomposite films with direction-dependent properties, Adv. Funct. Mater. 20 (2010) 429–436.
[29] Q. Wang, J.L. Mynar, M. Yoshida, E. Lee, M. Lee, K. Okuro, et al., High-water-content mouldable hydrogels by mixing clay and a dendritic molecular binder, Nature (2010) 463.
[30] A.K. Gaharwar, R.K. Avery, A. Assmann, A. Paul, G.H. McKinley, A. Khademhosseini, et al., Shear-thinning nanocomposite hydrogels for the treatment of hemorrhage, ACS Nano 8 (2014) 9833–9842.
[31] K. Haraguchi, Synthesis and properties of soft nanocomposite materials with novel organic/inorganic network structures, Polym. J. 43 (2011) 223–241.
[32] J.I. Dawson, J.M. Kanczler, X.B. Yang, G.S. Attard, R.O.C. Oreffo, Clay gels for the delivery of regenerative microenvironments, Adv. Mater. 23 (2011) 3304–3308.
[33] J.I. Dawson, R.O.C. Oreffo, Clay: new opportunities for tissue regeneration and biomaterial design, Adv. Mater. 25 (2013) 4069–4086.
[34] J.R. Xavier, T. Thakur, P. Desai, M.K. Jaiswal, N. Sears, E. Cosgriff-Hernandez, et al., Bioactive nanoengineered hydrogels for bone tissue engineering: a growth-factor-free approach, ACS Nano 9 (2015) 3109–3118.
[35] R. Rai, M. Tallawi, A. Grigore, A.R. Boccaccini, Synthesis, properties and biomedical applications of poly(glycerol sebacate) (PGS): a review, Prog. Polym. Sci. 37 (2012) 1051–1078.
[36] Y. Wang, Y.M. Kim, R. Langer, In vivo degradation characteristics of poly (glycerol sebacate), J. Biomed. Mater. Res., Part A 66 (2003) 192–197.
[37] Y. Wang, G.A. Ameer, B.J. Sheppard, R. Langer, A tough biodegradable elastomer, Nat. Biotechnol. (2002) 20.
[38] A.K. Gaharwar, A. Patel, A. Dolatshahi-Pirouz, H. Zhang, K. Rangarajan, G. Iviglia, et al., Elastomeric nanocomposite scaffolds made from poly (glycerol sebacate) chemically crosslinked with carbon nanotubes, Biomater. Sci. (2015).
[39] D. Motlagh, Jian Yang, K.Y. Lui, A.R. Webb, G.A. Ameer, Hemocompatibility evaluation of poly(glycerol-sebacate) in vitro for vascular tissue engineering, Biomaterials 27 (2006) 4315–4324.
[40] A.K. Gaharwar, M. Nikkhah, S. Sant, A. Khademhosseini, Anisotropic poly (glycerol sebacate)-poly (ε-caprolactone) electrospun fibers promote endothelial cell guidance, Biofabrication 7 (2015) 015001.
[41] S. Sant, D. Iyer, A.K. Gaharwar, A. Patel, A. Khademhosseini, Effect of biodegradation and de novo matrix synthesis on the mechanical properties of valvular interstitial cell-seeded polyglycerol sebacate–polycaprolactone scaffolds, Acta Biomater. 9 (2013) 5963–5973.
[42] R.A. Allen, W. Wu, M. Yao, D. Dutta, X. Duan, T.N. Bachman, et al., Nerve regeneration and elastin formation within poly (glycerol sebacate)-based synthetic arterial grafts one-year post-implantation in a rat model, Biomaterials 35 (2014) 165–173.
[43] Q.-Z. Chen, A. Bismarck, U. Hansen, S. Junaid, M.Q. Tran, S.E. Harding, et al., Characterisation of a soft elastomer poly(glycerol sebacate) designed to match the mechanical properties of myocardial tissue, Biomaterials 29 (2008) 47–57.
[44] J.M. Kemppainen, S.J. Hollister, Tailoring the mechanical properties of 3D-designed poly(glycerol sebacate) scaffolds for cartilage applications, J. Biomed. Mater. Res., Part A 94A (2010) 9–18.
[45] S. Redenti, W.L. Neeley, S. Rompani, S. Saigal, J. Yang, H. Klassen, et al., Engineering retinal progenitor cell and scrollable poly(glycerol-sebacate) composites for expansion and subretinal transplantation, Biomaterials 30 (2009) 3405–3414.
[46] S.H. Zaky, C.K. Hangadora, M.A. Tudares, J. Gao, A. Jensen, Y. Wang, et al., Poly (glycerol sebacate) elastomer supports osteogenic phenotype for bone engineering applications, Biomed. Mater. (2014) 9.
[47] A. Patel, A.K. Gaharwar, G. Iviglia, H. Zhang, S. Mukundan, S.M. Mihaila, et al., Highly elastomeric poly (glycerol sebacate)-co-poly (ethylene glycol) amphiphilic block copolymers, Biomaterials 34 (2014) 3970–3983.
[48] A.C. Tas, S.B. Bhaduri, Rapid coating of Ti6Al4V at room temperature with a calcium phosphate solution similar to 10× simulated body fluid, J. Mater. Res. (2004) 19.
[49] A.K. Gaharwar, A. Patel, A. Dolatshahi-Pirouz, H. Zhang, K. Rangarajan, G. Iviglia, et al., Elastomeric nanocomposite scaffolds made from poly(glycerol sebacate) chemically crosslinked with carbon nanotubes, Biomater. Sci. (2015) 3.
[50] T. Kokubo, H. Takadama, How useful is SBF in predicting in vivo bone bioactivity?, Biomaterials 27 (2006) 2907–2915
[51] P.J. Schexnailder, A.K. Gaharwar, R.L. Bartlett, B.L. Seal, G. Schmidt, Tuning cell adhesion by incorporation of charged silicate nanoparticles as cross-linkers to polyethylene oxide, Macromol. Biosci. 10 (2010) 1416–1423.
[52] A.K. Gaharwar, V. Kishore, C. Rivera, Wu.C.-J. Whitney Bullock, O. Akkus, et al., Physically crosslinked nanocomposites from silicate-crosslinked PEO: mechanical properties and osteogenic differentiation of human mesenchymal stem cells, Macromol. Biosci. 12 (2012) 779–793.
[53] A.K. Gaharwar, P.J. Schexnailder, B.P. Kline, G. Schmidt, Assessment of using Laponite cross-linked poly(ethylene oxide) for controlled cell adhesion and mineralization, Acta Biomater. 7 (2011) 568–577.